Journal of Materials Science Research and Reviews

2(4): 493-507, 2019; Article no.JMSRR.52208

Theoretical Investigations on Structural Stability and Elastic Properties of MoNbTaW-X (=Ti/V) High Entropy Alloys

A. Mishra[1*], G. Priyadarshan[1], D. Clark[1], Y. Lu[1] and Renhai Shi[2]

[1]Department of Mechanical Engineering, University of Mississippi, University, MS 38677, USA.
[2]Department of Materials Science and Engineering, The Ohio State University, 384 Watts Hall, 2041, USA.

Authors' contributions

This work was carried out in collaboration among all authors. Authors AM and DC designed the study, performed the statistical analysis, wrote the protocol and wrote the first draft of the manuscript. Authors AM, RS and GP managed the analyses of the study. Author YL managed the literature searches. All authors read and approved the final manuscript.

Article Information

Editor(s):
(1) Dr. Suraya Hani Bt Adnan, Associate Professor, Department Civil Engineering Technology, Faculty of Engineering Technology, Universiti Tun Hussein Onn Malaysia, Malaysia.
Reviewers:
(1) Miguel Jose Espitia Rico, Universidad Distrital Francisco José de Caldas, Colombia.
(2) Gavali Pankaj Balasaheb, Sanjay Ghodawat Institute, India.
(3) Hossam Ahmed Mohamed Halfa, Central Metallurgical R&D Institute (CMRDI), Egypt.
(4) Pasupuleti Venkata Siva Kumar, VNR VJIET, India.
Complete Peer review History: http://www.sdiarticle4.com/review-history/52208

Original Research Article

Received 04 September 2019
Accepted 11 November 2019
Published 16 November 2019

ABSTRACT

A refractory high entropy alloy based on MoNbTaW, with varying amounts of Ti and V, has been studied to elucidate the effect of the alloy composition on the electronic structure, phase stability, thermodynamic properties and the elastic properties. A synergistic approach has been adopted, employing empirical parameters, CALPHAD, and first principles calculations, to verify phase stability and single-phase solid solution formation for this alloy system. First-principles calculations are based on density functional theory, and employ the supercell method for modeling random alloys. The calculated lattice parameter for equiatomic MoNbTaW is in good agreement with available experimental data. The effect of Ti and V in various compositions on the electronic

**Corresponding author: Email: amishra2@olemiss.edu;*

structure of the host alloy has been elucidated via the density of states spectra. Elastic constants of C_{11}, C_{12}, and C_{44} of 9 alloys based on MoNbTaW with varying amounts of Ti and V, are reported by the stress-strain method and the Voigt-Reuss-Hill approximation. Elastic properties including Young's modulus, bulk modulus, Poisson's ratio and Debye temperature of polycrystalline alloys have been reported. All the alloys show mechanical isotropy for bulk modulus and Young's modulus. Addition of Ti and V in increasing amounts shows improved in ductility in the base alloy.

Keywords: Refractory high entropy alloys; CALPHAD; density functional theory; elastic constants; phase stability.

1. INTRODUCTION

Conventional multicomponent alloys are composed of one principal element and addition of alloying elements in trace amounts for improved strength and performance. However, most of these multicomponent alloys are still based on one principal element and are named after the principal elements, such as Fe-, Al-, Cu-, Ni-, and Ti-based alloys. Ni-base super alloys have become ubiquitous in the materials science community in the past half-century because of their superior ability to resist chemical and mechanical degradation at temperatures upwards of 70% of their melting temperatures. However, future generations of alloys with increased service lifetimes and higher efficiencies will require meeting specific materials specifications, such as high temperature creep resistance, oxidation resistance, and improved mechanical properties. High entropy alloys (HEAs) are being considered for use in high temperature applications and as coating material applications due to their unique combination of strength, ductility, thermal stability, corrosion and wear resistance.

HEAs contain at least five principal elements, the concentration of each element is between 5% and 35 at %. HEAs have higher entropy of mixing than traditional alloys, $\Delta S \geq 1.61R$ (R=8.314 J/mol.K), and form solid solutions with BCC/FCC by impeding the formation of intermetallic phases. Owing to their high entropy these alloys are believed to display: excellent anticorrosive properties, high hardness, high thermal stability, superior compressive properties, excellent wear resistance and unique magnetic properties [1,2,3,4], etc. these desirable properties make HEAs promising candidates for future engineering and industrial applications.

Interestingly, even with many elements mixed with a high concentration, simple phases such as solid solution [5,6,7] and sometimes, metallic glasses (MGs, or amorphous alloys) [8,9,10] tend to form in a large number of HEAs, without the formation of complex intermetallic compounds. Solid solution forming alloys have been developed in conventional alloys where there exists only one dominant element, and amorphous alloys used to be explored near eutectic compositions [11,12]. With the design concept of HEAs becoming more accepted by the materials community, more and more simple face-center cubic (FCC), body-center cubic (BCC), hexagonal close-packed (HCP) solid solution forming HEAs, and amorphous HEAs have been developed, some of which exhibit good mechanical [13,14,15,16] physical [17,18,19], chemical [20] and biomedical [10] properties. Therefore, HEAs provide new opportunities to design new alloys with potentially new properties.

Structural and mechanical properties of HEAs based on refractory metals have been a popular configuration for many researchers due to their high melting temperatures [21,22]. Metallic alloys used in waste incinerators, turbines and space applications are currently limited to operating temperatures of around 135ºC; the upper stability limit of many NiAl super alloys. However, solely using refractory metals carries the downside of high density. Therefore, additional elements such as Hf, Zr, Cr and Ti are added or substituted into the alloy in order to create a more practical material [23] [24,25,26]. Various concentrations of Al have also been added in order to decrease weight and form oxide scales to enhance the corrosion resistance of the alloy [25,27]. Combinations of the aforementioned elements are of relative atomic size and the enthalpies of formation of the binaries are similar which generally lead to a simple BCC phase often with a dendritic structure, which can be homogenized with proper annealing [25]. The refractory base elements exhibit BCC crystal structures and less ductility than most FCC elements; however, Senkov, et al. [28] reported a room

temperature, true strain of 2.3 for HfNbTaTiZr showing that a simple weighted average approach of base elements is not completely accurate when describing toughness and ductility.

Senkov, et al. [21] have also reported the development and characterization of refractory alloys based on W, Nb, Mo, Ta, and V. B. Gorr et al. discussed a refractory high entropy alloy system MoWAlCrx high temperature structural applications, with excellent oxidation resistance [27]. Chien-Chang Juan, et al. [29] discussed two new alloys with simple BCC structure, HfMoTaTiZr and HfMoNb-TaTiZr. Senkov et al. [22,30,31,27,29] studied two refractory HEAs based on NbMoTaW.

Huhn, et al. [32] pointed out two properties of high entropy alloys that warrant research in the field: cocktail effects and simple lattice stability at elevated temperatures. Cocktail effects were discussed by Yeh [33] as one of the four core effects of multicomponent alloys. The importance of this effect is that each individual constituent will ultimately confer its properties to the overall behavior of the system. Like the philosopher's stone to alchemy, the ability to tailor a material to a specific application is a paradigm shift in material design. In the past, materials such as copper, stainless steel and vulcanized rubber were discovered unintentionally and uses were found at a later time. Coupled with today's processing power and accurate potentials, properties can be optimized using computers by varying compositions slightly. Simple lattice stability, the second important property, is crucial for carrying out these calculations. High entropy alloys often exhibit simple BCC, FCC or HCP structures, rather than complex intermetallic phases. Even in cases where multiple phase regions exist, the phases themselves tend toward simple Im3m or Pm3m space groups [33]. Several computational methods have ben used to predict the electronic, thermodynamic and mechanical properties of high entropy alloys. These methods include the CALPHAD (CALculation of Phase Diagrams [34] approach, first principles/ab-initio methods, and molecular dynamics simulations.

Density functional theory (DFT) is a widely accepted ab initio method and has been extensively applied to calculate the electronic properties of materials. According to the theorem of [35] the ground state of a system is described via the energy functional. DFT is a quantum mechanical modeling technique that essentially solves the Schrodinger equation in order to explain how a system will evolve. The advantage of DFT is that it works with density as a function of position rather than the wave function, which depends on the position of every particle as well as an electron spin. The density-functional perspective is therefore quite different than the many-body perspective. When modeling a HEAs, the number of electrons can get very large and thus replacing the wave function with ρ(r) speeds up calculations.

DFT differs from molecular dynamics (MD) in that atomic interactions and total energy of the system is found by approximating solutions to the Schrodinger equation. Reaction dynamics can be observed since electrons are taken into consideration. However, MD neglects quantum effects and calculates energy and reactions by approximating the atoms as classical particles. While this reduces computation time, accuracy is lost by neglecting the wavelike nature found on the atomic scale. Also, accurate classical potentials are difficult to come by when simulating exotic materials.

Gao, et al. have successfully used ab-initio method based on molecular dynamics method (AIMD) to predict the single-phase solid solution of FCC alloys based on 3d transition elements, and BCC alloys based on refractories [36,37]. The AIMD method does not rely on interaction potentials, which is essential for molecular dynamics simulations. Special quasi-random structure (SQS) [38] and coherent potential approximation (CPA) [39] are techniques widely employed in the first-principles calculations of random alloys. The idea of SQS is to construct a special supercell of which the atomic correlation functions mimic those of the physically most relevant ones of the perfectly random alloys. Within the supercell, the atomic positions may be relaxed through minimizing the interatomic Hellmann– Feynman forces during the first-principles calculations such that the local lattice distortion effect induced by alloying atoms is taken into account. This is the main advantage of SQS over other mean field approximations such as VCA and CPA. However, the size of the supercells needed for multi-components alloys (e.g. non-equiatomic high entropy alloys [2,40] can eventually become of limiting factor for the SQS approach. The symmetry of the SQS supercell is generally very low due to the quasi-random distribution of the atoms. This makes the

calculations of some symmetry dependent properties inconvenient. In particular, the number of independent elastic constants Cij increases greatly due to the lowering of the lattice symmetry. Virtual Crystal Approximation is another mean-field scheme for random alloys [41]. Different from CPA, the VCA effective medium is represented by the composition weighted individual pseudoptentials of the alloy components. It has been recognized that VCA is applicable only to those systems where the alloying components have similar electronic configurations (systems consisting of elements with atomic numbers close to each other or belonging to the same group of the periodic table).

In this study we use the CALPHAD method along with first principle DFT calculations to predict single-phase solid solution of BCC alloys based on MoNbTaW-X, where X is Ti and V. The amount of Ti and V is varied from (0-33 atomic %), while altering the concentration of Mo. Nb, Ta, and W. We calculated electronic structure, phase stability, elastic properties, lattice parameter, and thermodynamic properties for 9 different alloy systems with varying concentrations of Ti and V in the host alloy MoNbTaW, based on the CALPHAD method and first principles calculations. Because of the proximity of the elements in the periodic table, we first utilized the VCA approximation to model ransom alloys, but got erroneous results and have not included the data in this work. It should be noted that in the present study the we are not using the SQS or the CPA methods in this work have not been utilized. but rather proving This work relies on the efficacy of coupling CALPHAD with DFT (utilizing supercell method) results, while relying on empirical rules established for HEAs and available experimental data. The aim of this work is to provide design rules for solid-solution phase formation of refractory high entropy alloys based on MoNbTaW, and predicting their elastic properties with respect to varying alloy concentrations. Although MoNbTaW systems have been theoretically and experimentally studied, we chose this specific alloy in order to prove the efficacy of above mentioned methods, and compare our results with available data. The main goal of this work is to employ these methods to study the effect of alloying on the electronic structures, phase stability, and elastic properties of refractory high entropy alloys based on MoNbTaW with an aim to ductilize the alloy while reducing the density.

2. METHODOLOGY

2.1 Atomic Size Difference, Electronegativity Difference, and Valence Electron Concentration

Prior to performing DFT calculations for determining elastic constants, we considered the possibility of the refractory alloys, actually forming solid solutions. Since our hypothesis and calculations are based on the eventuality of the (MoNbTaW)xTi(1-x) and MoNbTaWxV(1-x) systems forming single phase solid solutions, we factored the thermodynamics of the binary systems comprising the multicomponent alloy. Although Hume-Rothery rules are a good starting point, we noticed that the difference in atomic size for Ta and V is 16.9%. All other binary pairs fall within the specified limit. It was also determined that there were no large differences in electronegativities. While there is no strict adherence to the Hume-Rothery rules, HEAs do not necessarily have to meet all the criteria in order to form a solid solution.

The atomic size difference is denoted by the $\delta\rho$ parameter, and is defined as:

$$\delta r = 100\% \sqrt{\Sigma_{i=1}^{N} \left(1 - \frac{r_i}{\Sigma_{j=1}^{N} c_j r_j}\right)^2} \quad (1)$$

where r_i and r_j is the atomic radius of the i^{th} an j^{th} element. As reported, a small value of $\delta\rho$ is desirable for large solubility (less than 6 for single phase solid solution formation) [4]. However, such an estimation is somewhat abstruse since the same atomic species in different systems may show different atomic radii and several different definitions of the atomic radii exist.

We have considered the difference in electronegativity as well. The difference in electronegativity can be calculated by the following formula:

$$\delta\chi = 100\% \sqrt{\Sigma_{i=1}^{N} \left(1 - \frac{\chi_i}{\Sigma_{j=1}^{N} c_j \chi_j}\right)^2} \quad (2)$$

Guo, et al. [42] have related valence electron concentration (VEC) of HEA compositions to their crystal structure. Their research yielded the observation that for HEAs with a VEC less than 6.87 the solid solution formed had a bcc crystal structure, those with VEC greater than 8 formed fcc solid solutions and alloys with

intermediate VEC formed a mixture of bcc and fcc solid solutions.

$$VEC = \Sigma_{i=1}^{N} c_i VEC_i \quad (3)$$

where c_i is the composition of i^{th} element, and VEC_i is the valence electron concentration of individual elements.

2.1.1 Mixing enthalpy consideration

Troparevsky, et al. [43] proposed a simple predictive method, which solely relies on enthalpy of formation data to determine which elements will combine to form single-phase alloys. Specifically, if every binary's enthalpy of formation falls within a set range, a single phase is expected. Enthalpy of formation data can be found in alloy databases or calculated using computational methods such as DFT. Most elemental pairs have negative enthalpies of formation indicating an exothermic process. Complex compounds are unlikely to form in HEAs due to slow diffusion of the alloying elements under proper annealing, therefore, it is reasonable to consider only the binaries. The method proposed by Troparevsky, et al. accurately predicts single phase HEAs that have been experimentally proven and rejects systems that form intermetallics or multiple phases. The range that binaries must fall into in order to form a single phase is set by $-T_{ann}\Delta S_{mix}$ and the largest value of ΔH_f for which the alloy does not show phase separation. This range ensures that the system is neither too stable in which compounds could precipitate, nor unstable in which the constituent elements would not mix at all. Specifically, the upper range is 37meV and is chosen as it includes all known single-phase alloys. Both the lower and upper limits are justified as follows: solid solution alloys with multiple components typically show small enthalpies of formation and ordered compounds generally present small entropic terms. As stated above, only data from binary combinations need to be calculated and fall within the given range.

For modeling considerations, the annealing temperature to set the minimum value of the range can be approximated by substituting a critical temperature for the annealing temperature. This critical temperature can be approximated as $.6T_m$, where T_m is the average melting temperature of the constituent elements. Taking this specific fraction of the average melting temperature is consistent with experimental annealing temperatures [43]. Assuming $.55T_m$ is equivalent to T_{ann} for a tighter range of mixing enthalpies. T_{ann} is then equal to 1452°C for the MoNbTaTiW system when using the average melting temperatures for T_m. To find the value for mixing enthalpy $\Delta H_{mix} = -T_{ann}\Delta S_{mix}$, the equation below can be used.

$$\Delta S_{mix} = -nR\ \Sigma_i\ (c_i \ln c_i) \quad (4)$$

Where n is number of constituent elements, and c_i is the composition of each element in the alloy.

Granting that low values of, δr, and large values of $\Omega \left(= \frac{T_m \Delta S_{mix}}{\Delta H_{mix}}\right)$ have a tendency to form solid solutions, empirical parameters by themselves are not sufficient criteria. Moreover, these empirical parameters predict a range of values for solid solution phase formation, which are dependent on experimental data. This can prove to be restrictive, and to overcome this, a combined approach of analyzing existing binary phase diagrams, CALPHAD, first-principles density functional theory (DFT), and ab-initio molecular dynamic simulations.

2.2 CALPHAD Modeling

Phase diagrams provide information about what microstructures are to be expected when different elements are brought together under varying temperatures and pressures. Mo, Nb, Ta, and W crystallize in the BCC_A2 phase at room temperature. CALPHAD (Calculation of Phase Diagrams) [44] has been established as an effective technique for the prediction of phase equilibria of multicomponent systems, based on the binary and ternary phase diagrams. Senkov, et al. [45,46,47] have established the efficacy of CALPHAD calculations based on the thermodynamic assessment of fully assessed binary and ternary systems. They theorized that the formation of novel quaternary intermetallics is highly unlikely, since quarternary and higher order interactions are negligible.

If each of the elements were to be alloyed, it is highly unlikely that a phase would exist that is not present on the diagrams. Fig. 1 shows the Mo-Nb, Mo-Ta, Mo-W, Nb-Ta, Nb-W, and Ta-W binary phase diagrams, which show that the BCC_A2 phase (Im3m)is stable over a wide composition range. Experimental data reported in the literature also suggests the formation of a stable single solid solution phase for MoNbTaW high entropy alloy, which further strengthened our assumptions that the MoNbTaW system forms a single phase solid solution [21,22].

There are also experimental studies on of (MoNbTaW)xTi(1-x), which confirm the formation of a single phase solid solution [48,49]. The constituent binary phase diagrams, for this alloy system is shown in Fig. 2. Mo, Nb, Ta, and W stabilize in the BCC_A2 phase at ambient conditions, whereas Ti stabilizes in the HCP phase. But Ti stabilizes in the BCC_A2 phase at high temperatures. As can be seen in Fig. 2, Mo-Ti, Nb-Ti, Ta-Ti, and W-Ti binary phase diagrams all show a wide BCC_A2 region, and do not show the formation of intermetallic phases.

Binary phase diagram for the Mo-V, Nb-V, Ta-V, and W-V phase diagram are shown in Fig. 3. The Nb-V, and the W-V binary system shows the presence of a miscibility gap, whereas, the Ta-V binary shows the presence of laves phases. In order to determine the possibility of a single phase solid solution in the (MoNbTaW)xV(1-x) system, we used the TCHEA3 database in ThermoCalc to predict the phase formation of this system. We also use the database to predict phase formation for the (MoNbTaW)xTi(1-x) alloy. The results are discussed n the next section.

CALPHAD calculations were carried out mainly using the TCHEA3 thermodynamic database via the ThermoCalc^{TM} software [50] on equi-molar compositions MoNbTaWTi, and MoNbTaWV.

2.3 Density Functional Theory

In order to account for the distribution of local chemical environment in random solid solution formation, we utilized the supercell method. The supercell method is expected to take into consideration the random distribution of alloying species, long-range order, short-range order, partial order, etc. We first constructed a supercell based on the BCC_A2 structure as evidenced from the binary phase diagrams of the constituent elements in the alloys.

In this method, one first constructs the large supercell based on the unit cell of crystal structure, then makes the alloying elements randomly distribute on the lattice sites. Based on the BCC_A2 (Im3m) symmetry unit cells, the modeled systems including 54 and 48 atom supercells for the fully disordered and partial-order hexagonal Mo-Pd-Rh-Ru-Tc HEAs, respectively. King, et al. [51] showed that these sizes are sufficient to achieve convergence in total energy. Results suggested that single phase solid solutions are predicted to transform to a partial-order structure [51,52].

Due to the large number of possible arrangements, we constructed 5 supercells for each alloy system. We changed the concentration of Ti and V in MoNbTaWTi and MoNbTaWV respectively from 0-33%. The exact number of atoms used had to be adjusted depending on the concentration of titanium or vanadium that was being investigated. It was not possible to represent titanium/vanadium at 11.1%, 20%, 25%, etc. in the same sized cell. For each supercell, the equimolar Mo, Nb, Ta, and W alloying elements were randomly assigned to the lattice sites. Via the geometrical optimization based on ab initio calculations, the energy per MoNbTaW system varied by ±0.15 eV for most of configurations. The average energies are acceptable considering the variation in arrangement between each supercell, whereas both vacancy formation energy and defect energy strongly depend on the alloying elements [51].

The number of atoms used in each simulation needs to be enough so that the cell is representative of a random solid solution, yet not too large as to be computationally expensive. In order to find the optimum size, various sized supercells of MoNbTaW were simulated and the elastic moduli plotted to find the convergence point. The alloy is expected to be isotropic and thus, the Young's modulus in each of the Cartesian coordinate directions should be very similar in value. From the plot, the x, y, and z values all converge to approximately 295 GPa, as the number of atoms in the system exceed 16. To ensure convergence of the elastic moduli, all subsequent simulations were performed on supercells with at least 16 atoms. The exact number of atoms used had to be adjusted depending on the concentration of titanium or vanadium that was being investigated. It was not possible to represent titanium at 11.1%, 20%, 25%, etc. in the same sized cell. For example, to represent titanium at 25% required a ratio of 4:3:3:3:3 in $MoNbTaWTi_{25}$.

Metals and alloys, including high entropy alloys, are expected to exhibit linear elasticity. If theoretical calculations show behavior that is not consistent with this notion, then Hooke's Law is not applicable and the data is not valid. The quasi-static strain amplitude was adjusted multiple times and the modulus of elasticity did not change for MoNbTaW, MoNbTaWTi or MoNbTaWV. Specifically, the maximum strain

amplitude was varied between 0.003, 0.03 and 0.3 without any effect on the elastic properties. All of the simulations were performed with a quasi-static strain amplitude of .03 to ensure that the material was in the linear elastic range. The Young's modulus varied only slightly when the atoms were placed in different positions.

Convergence criteria for the geometry optimization were less strict than the elastic constant calculations as the weighted average approach for the lattice parameter proved to be quite accurate. As a result, the geometry optimization only changed the lattice parameter of the system by 1-2% regardless of the convergence tolerances. The atomic positions were fixed and only the cell was altered to find equilibrium. The basis set for the variable cell was set to fixed basis quality and the compressibility was set to hard. No external stress was applied. Elastic simulations used an ultrasoft pseudopotential represented in reciprocal space. The maximum cutoff energy was set to $2x10^{-5}$ eV/atom.

The unit cell was achieved through a close structure as shown in Fig. 1. The total energy code Cambridge sequential total energy package (CASTEP) was used for all the calculations. Geometrical optimization was performed to obtain the theoretical equilibrium crystal structure of the alloy systems. The lattice constant and internal atomic coordinates were optimized independently to minimize the free enthalpy, inter-atomic forces and unit cell stresses. Within the first-principles calculations, the interaction between the ion cores and the electrons was represented by the Vanderbilt-type ultra-soft pseudopotential. The electronic exchange-correlation energy was treated under the generalized gradient approximation (GGA). The plane-wave basis set cutoff was set to 450 eV for all the calculations. Special points sampling integration over the Brillouin zone was employed by using the Monkhorst–Pack method with a 3x3x3 special k-points mesh. The Brodyden-Fletcher-Goldfarb-Shanno (BFGS) minimization scheme was used in geometrical optimization. The convergence criteria for the geometrical optimization are that the difference in total energy is within $2x10^{-5}$ eV/atom, the maximum ionic Hellmann–Feynman force is within 0.01 eV/Å, the maximum ionic displacement is within $5x10^{-4}$Å, and the maximum stress is within 0.02 GPa. These parameters lead to good convergence of the total energy and geometrical configuration.

Table 1. Atomic size difference, electronegativity, crystal structure, lattice parameter, density, and melting temperature of constituent elements

	Atomic size (Å)	χ	Crystal structure	Lattice parameter (Å)	Density (g/cm3)	Melting temperature (^{0}C)
Mo	1.90	2.16	BCC	3.14	2.16	2617
Nb	1.98	1.60	BCC	3.30	1.60	2468
Ta	2.00	1.50	BCC	3.30	1.50	2996
W	1.93	2.36	BCC	3.16	2.36	3410
Ti	1.76	1.54	HCP	3.96	1.54	1660
V	1.71	1.63	BCC	3.03	1.63	1890

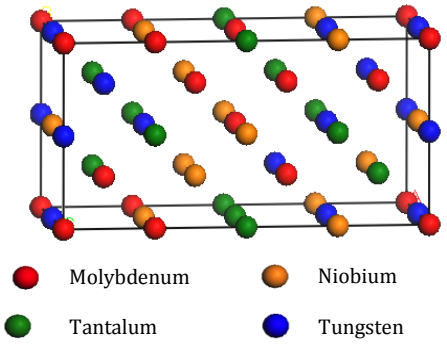

Fig. 1. Schematic of a unit cell used for DFT calculations

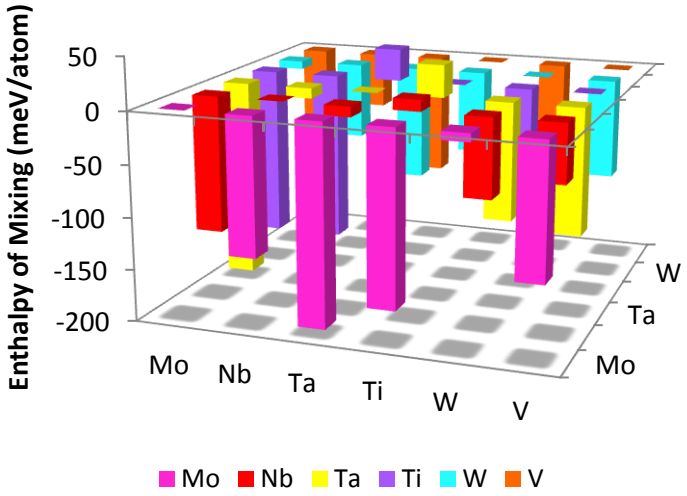

Fig. 2. Enthalpies of mixing for binary systems

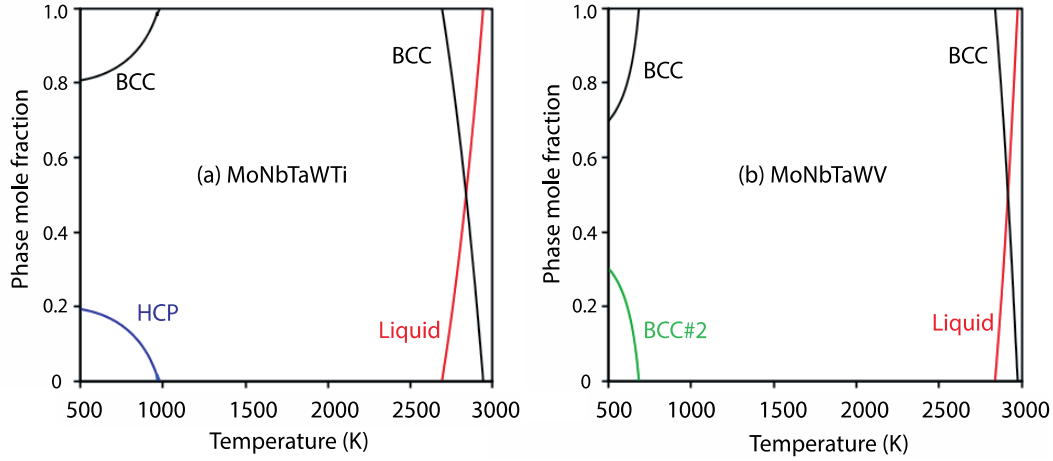

Fig. 3. Equilibrium phase mole fraction versus temperature for (a) MoNbTaWTi, and (b) MoNbTaWV predicted from TCHEA3 database

3. RESULTS AND DISCUSSION

3.1 Alloy Parameters Based on Empirical Rules

Based on the empirical rules considered in this work, the valence electron concentration, atomic size mismatch, difference in electronegativities, and ΔS_{mix} have been calculated and are presented in Table 3. The VEC shows a downward trend with the addition of increased amounts of Ti/V in the base alloy.

The S_{mix} for a system of 5 constituent elements in equal atomic proportion is equal to 0.1387 after converting to units of meV/K-atom. Finally, solving $-T_{ann}\Delta S_{mix}$ yields a lower limit of -201.4 meV/atom. Therefore, every binary combination should have a mixing enthalpy that falls within the range of -201.4 meV < ΔH_{mix} < 37 meV. Indeed, all of the binaries for the MoNbTaWTi alloy fall within this range as can be seen in Fig. 2. Note that all of the binaries are within the range when substituting titanium with vanadium.

3.2 Calphad Modeling

Equi-molar compositions for both MoNbTaWTi and MoNbTaWV alloy systems have been studied via CALPHAD methodology using TCHEA3 database with Thermo-Calc software. For MoNbTaWTi alloy, the equilibrium phase diagram has been calculated and predicted the equilibrium relationship of various phases shown in Fig. 3(a). It suggests that BCC phase is

thermodynamically stable between 955K and 2681K. Above 2681K, the liquid phase will appear with dissolving BCC. Also, the HCP phase will precipitate when heat treatment temperature is below 955K. The classic Scheil model is used to calculate the solidification sequence and simulate the solidified microstructure of MoNbTaWTi alloy shown in Fig. 3(b). The resulting calculation shows that only BCC phase will be solidified after the solidification.

For MoNbTaWV alloy, the equilibrium calculation has been performed and shown in Fig. 3(a). The BCC phase is predicted to be stable between 759K and 2717K, which shows wider thermal window (ΔT=1958) than one (ΔT=1726) of MoNbTaWTi alloy for thermal stability of BCC phase. The liquid phase will be observed starting from 2717K and the ordered BCC phase will also appear when the temperature is below 759K. The solidification sequence of MoNbTaWV alloy has also been calculated via the classic Scheil Model and shown in Fig. 3(b). The result suggests that the solidified matrix will only consist of BCC phase after the solidification, which is similar to MoNbTaWV alloy.

3.3 Effect of Alloying on Electronic Structure of MoNbTaW Host Alloy

In order to analyze the effect of alloy chemistry on MoNbTaW, we have calculated the electronic density of states (DOS) for MoNbTaW-X (x=Ti/V from 0-33%). For brevity we have reported the DOS and PDOS spectra of MoNbTaW, MoNbTaWTi, and MoNbTaWV in equiatomic proportions. The results are shown in Fig. 4(a). Since the elements are situated in close proximity in the periodic table, the total DOS of these alloys are similar. The DOS of pure elements have also been plotted. For Ti, a large peak is located near the Fermi level, which is agrees with the fact that Ti is stable in the HCP structure, and unstable in the BCC phase. In a cubic lattice the d states are degenerated, which have a tendency of splitting in the event of lattice distortion. The additional electrons in V and Nb shift the Fermi level towards a decreasing DOS and finally reaches the characteristic minimum in BCC Mo and W. The total and partial DOS of MoNbTaW, MoNbTaWTi, and MoNbTaWV are show in Fig. 4(b) and (c) respectively. Due to the loss of structural characteristics of the DOS and PDOS of the alloys as compared to elemental DOS, only broad peaks are evident near the Fermi level for all the alloys. The total DOS curves for alloys containing Ti and V display a shift of the peak towards the Fermi level. The peak nearest to the Fermi level shifts closer with the increase of V and Ti, to the MoNbTaWV and MoNbTaWTi alloys respectively, which is consistent with the PDOS of alloys, and elemental DOS.

The PDOSs are somewhat different from the DOSs of the elemental metals. In all three cases, Ta and Nb contribute with a peak to the DOS at the Fermi level. The partial DOS is very similar to the pure metal DOS in MoNbTaW. The partial DOS of Mo is strongly altered compared to that of pure Mo. However, the presence of Mo makes the V and Nb partial DOS more V- and Nb-like, respectively (where the Fermi energy shows a downward trend).

The effect of alloy chemistry changes the bulk modulus of alloys. Generally, the larger volume the alloy has, the smaller bulk modulus is expected. We observe that the host alloy MoNbTaW has similar bulk modulus to alloys containing low concentrations of Ti and V. There is a slight initial increase in V containing alloys, for V=11-20%, then the bulk modulus decreases. For Ti containing alloys, the bulk modulus shows a decreasing trend with high concentration of Ti. This shows that higher concentrations of Mo,Ta, and W yield higher bulk modulus. The bulk moduli of metallic Mo, Ta, and W, are 2–3 times larger than that of metallic Ti, Zr, Hf and Nb. Therefore, it is expected that alloys containing higher concentrations of Mo, Ta, or W increases the bulk moduli of MoNbTaWX(X=Ti/V) systems.

The elastic constants of bcc equimolar MoNbTaWX are shown in Fig. 5. Alloys based on Mo, Ta, and W, much larger C_{11} compared to other systems, and therefore, their Young's moduli are also large. MoNbTaW has a C_{11} of 383.97 GPa, and its Young's modulus is 290 GPa.

3.4 Elastic Properties from DFT Calculations

The knowledge of elastic constants is vital for many practical applications related to the mechanical properties of a solid. This is a very significant property to study mechanical properties like ductility and stiffness. Several theoretical models have been developed for the determination of elastic constants. In the present

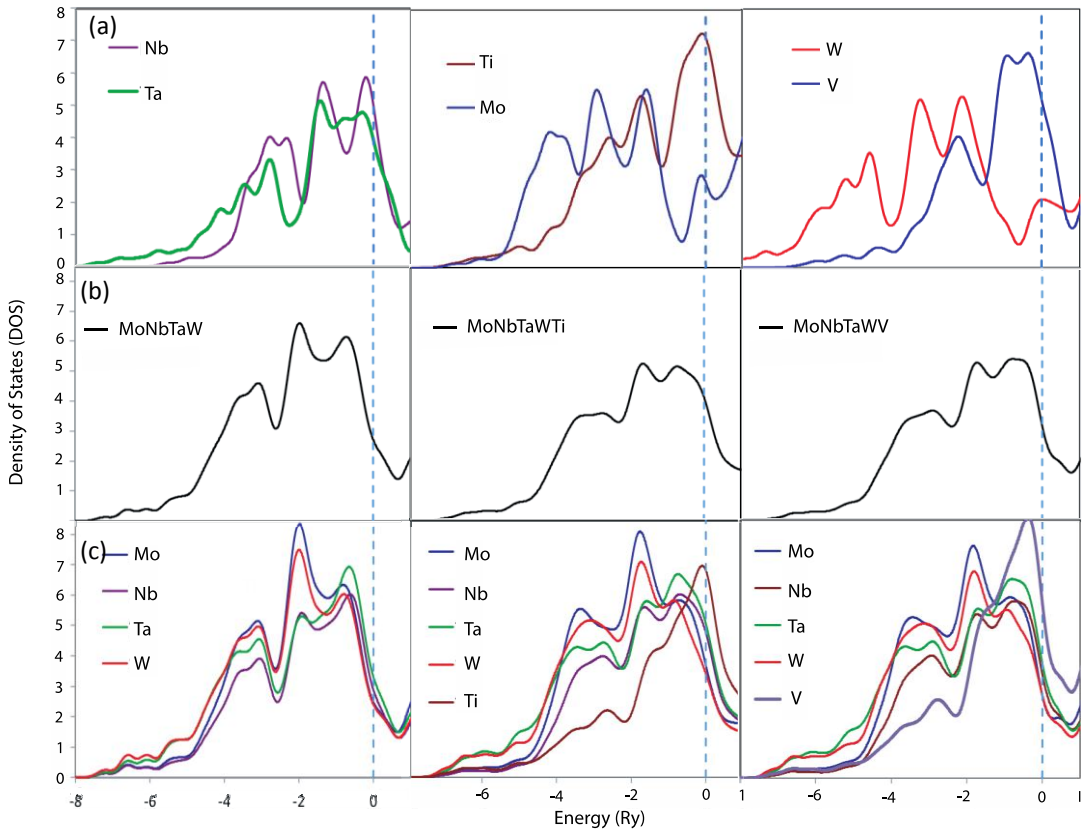

Fig. 4.(a) Elemental density of states (DOS) spectra for Nb, Ta, Ti, Mo, W and V (top section), (b) DOS and (c) PDOS for MoNbTaW, MoNbTaWTi and MoNbTaWV equiatomic alloys

study, we have used the theoretical model of Charpin [53] to determine the elastic constants of the refractory alloys. The alloys in this study are determined to possess a cubic symmetry, hence three elastic constants, C_{11}, C_{12}, and C_{44}, are to be calculated. The value of these elastic constants was obtained by calculating the total energy as a function of volume-conserving strains and is presented in Table 2. As far as the criteria for cubic elastic constants are concerned our predicted values (Table 3) well satisfy the following criteria:

$$(C_{11} - C_{12}) > 0 \quad (5\text{-a})$$

$$C_{11} > 0,\ C_{44} > 0 \quad (5\text{-b})$$

$$(C_{11} + 2C_{12}) > 0 \quad (5\text{-c})$$

$$C_{12} < B < C_{11} \quad (5\text{-d})$$

Poisson's ratio (v), Young's modulus (E), and shear modulus (G) are often measured for materials when their hardness is to be investigated. These quantities are calculated from the computed data of the elastic constants by using the following expressions [54] and presented in Table 3.

$$\nu = \frac{(3\,B - 2\,G)}{2\,(3\,B + G)} \quad (6)$$

$$E = \frac{9BG}{3B+G} \quad (7)$$

where B is the bulk modulus and G is the average shear modulus. As per Hill [54], the average shear modulus, G, is defined as the arithmetic mean of Voigt, G_V , and Reuss, G_R , [55,56] values, which can be calculated as:

$$G_V = \frac{1}{5}(C_{11} + C_{12} + C_{44}) \quad (8)$$

$$G_R = \frac{5(C_{11}-C_{12})C_{44}}{3(C_{11}-C_{12})+4C_{44}} \quad (9)$$

$$A = \frac{2C_{44}}{C_{11}-C_{12}} \quad (10)$$

The Zener anisotropy for the alloys is more than 1; consequently the material does not display anisotropic behavior.

The ductility and brittleness of the alloys can be defined by the B/G ratio. According to Pugh [57],

a material is brittle if the B/G ratio is less than a limit value of 1.75 and is ductile if it is higher than this limit value. The B/G ratio for the alloys is calculated to be in the range of 2.07-2.9, which is higher than the limit value; thus the alloys show a ductile nature. Increasing the V and Ti content seem to increase the ductility of the alloy. It is well known that Cauchy pressure (C_{12}–C_{44}) [48] can also indicate the ductile or brittle nature of an alloy. A negative Cauchy pressure indicates

Table 2. Calculated elastic constants C_{11}, C_{12}, and C_{44} of MoNbTaWTi$_x$ and MoNbTaWV$_x$

Alloy composition	C_{11}	C_{12}	C_{44}	ρ (g/cm^3)	VEC	a (Å)	δ_ρ	$\delta\chi$
MoNbTaW	383.97	158	111.97	13.68	5.5	3.264	2.32	38.18
$(MoNbTaW)_{89}V_{11}$	373.85	152.3	110.33	12.84	5.4	3.214	2.06	40.87
$(MoNbTaW)_{80}V_{20}$	346	146	97	12.17	5.4	3.191	1.83	41.50
$(MoNbTaW)_{75}V_{25}$	310.42	135	82	11.79	5.3	3.179	1.71	41.85
$(MoNbTaW)_{67}V_{33}$	295.43	136	72	11.161	5.3	3.162	1.50	42.55
$(MoNbTaW)_{89}Ti_{11}$	353.33	148.2	99.98	12.66	5.3	3.314	2.26	40.96
$(MoNbTaW)_{80}Ti_{20}$	283.44	130.5	74.73	11.85	5.2	3.383	2.20	41.97
$(MoNbTaW)_{75}Ti_{25}$	286.47	132	74.73	11.39	5.1	3.415	2.17	42.57
$(MoNbTaW)_{67}Ti_{33}$	236.66	128	58.13	10.62	5.0	3.254	2.12	43.80

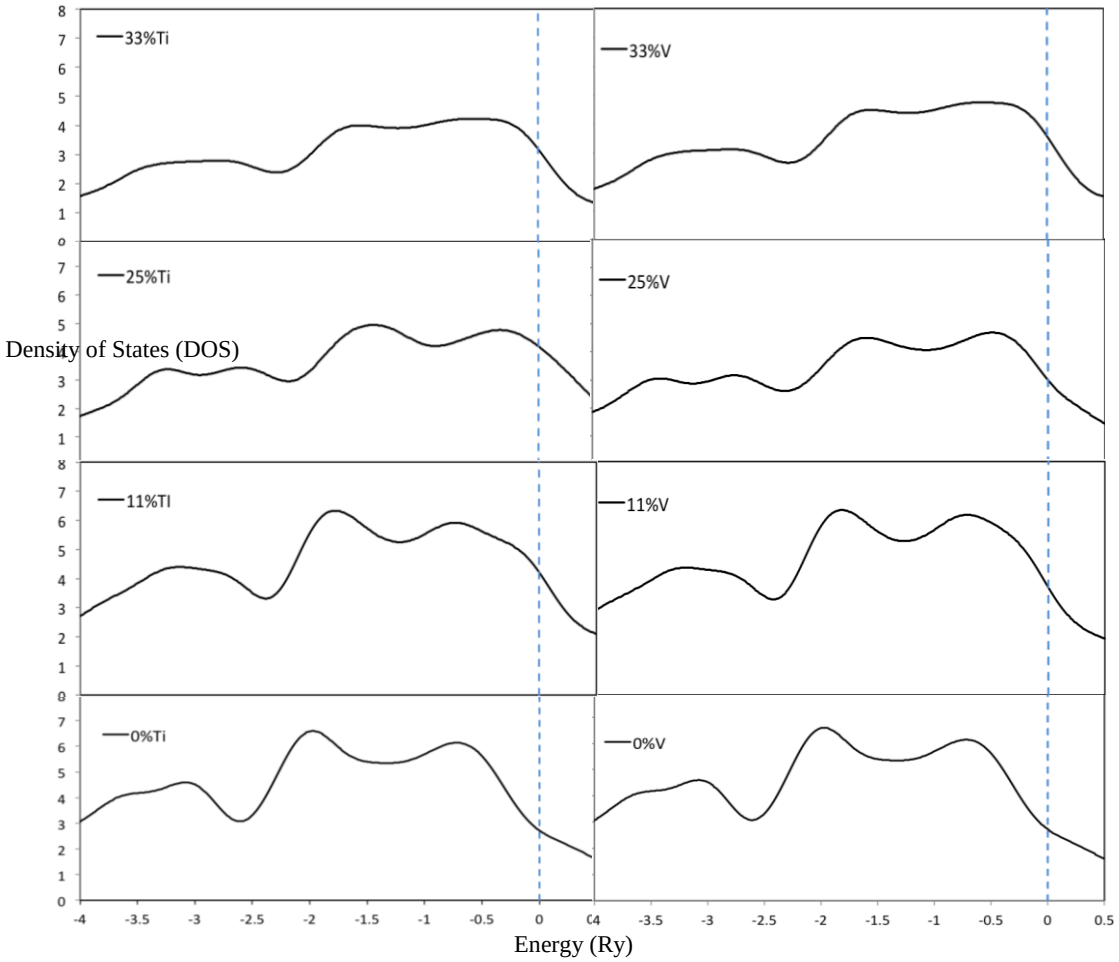

Fig. 5. DOS spectra of MoNbTaW alloy with varying concentrations of Ti and V (0-33 at. %)

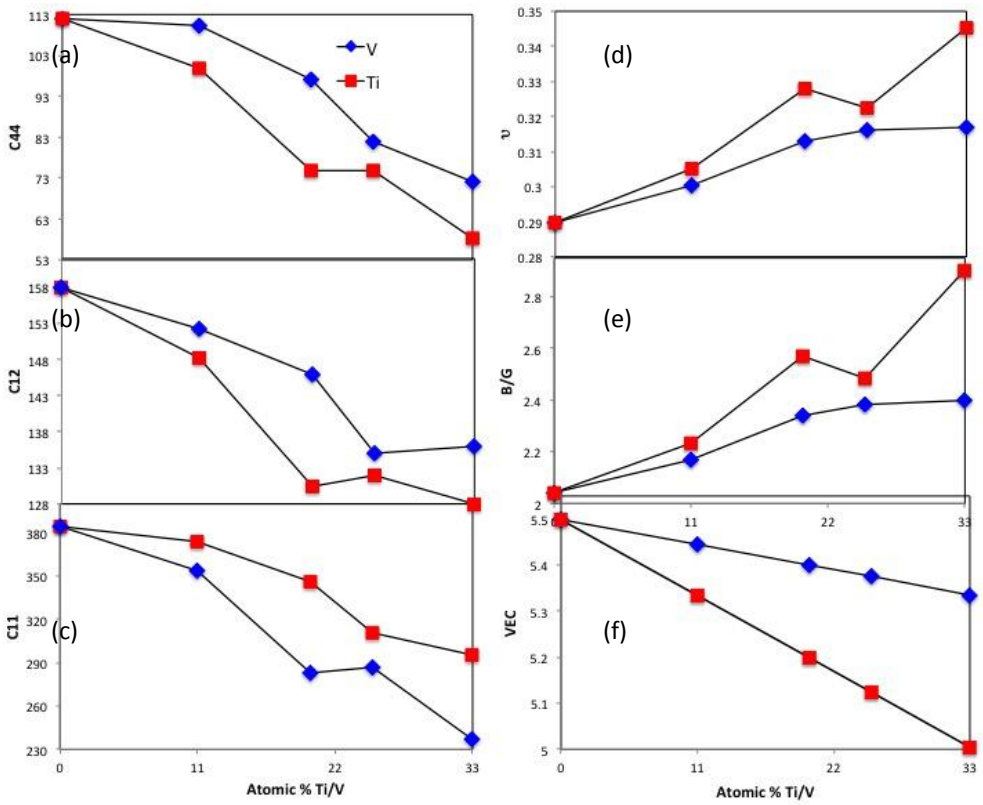

Fig. 6. Plots of (a) C_{44} (GPa), (b) C_{12} (GPa), (c) C_{11} (GPa), (d) Poisson's ratio (ν), (e) Pugh's ratio (B/G), and (f) valence electron concentration (VEC), vs. percent increase of Ti and V in MoNbTaW alloy

Table 3. Calculated values of shear modulus G (GPa), Young's modulus E (GPa), Poisson's ratio ν, Zener anisotropy factor A, B/G ratio, Cauchy pressure C_{12}-C_{44}, and θ_D in Kelvin

Alloy	G (Gpa)	E (GPa)	B(GPa)	υ	Az	B/G	C_{12}-C_{44}	θ_Δ (K)
MoNbTaW	110.53	294	229.5	0.29	0.98	2.04	46.26	412
$(MoNbTaW)_{89}V_{11}$	108.27	288	240	0.31	0.99	2.17	41.97	421
$(MoNbTaW)_{80}V_{20}$	81.20	216	230	0.32	0.98	2.34	47.15	409
$(MoNbTaW)_{75}V_{25}$	71.80	191	200.8	0.32	0.99	2.41	48.13	383
$(MoNbTaW)_{67}V_{33}$	66.16	176	179.8	0.35	0.97	2.45	45.98	372
$(MoNbTaW)_{89}Ti_{11}$	81.20	216	225.5	0.31	0.99	2.23	46.13	402
$(MoNbTaW)_{80}Ti_{20}$	70.67	188	193.9	0.32	1	2.57	54.03	356
$(MoNbTaW)_{75}Ti_{25}$	63.90	170	188	0.33	0.98	2.48	60.26	362
$(MoNbTaW)_{67}Ti_{33}$	56.39	150	164.1	0.34	0.97	2.90	59.86	322

brittleness due to directionality of bonding, while positive values of C_{12}–C_{44} indicate ductlity [58]. Pugh's rule can also used to express ductility using Poisson's ratio so that alloys with $\nu > 0.29$ are ductile and those with $\nu < 0.29$ are brittle. According to these rules, all combinations from Table 3 are predicted to be ductile at room temperature.

Heat capacities of solids can be understood by calculating the Debye temperature θ_Δ. Debye temperature can be calculated from the elastic constant data, as θ_Δ can be estimated from the average sound velocity, v_m, by the following equation:

$$\theta_D = \frac{h}{k_B}\left[\frac{3}{4\pi V_a}\right]^{1/3} v_m \qquad (11)$$

where h is Planck's constant, k_B is Boltzmann's constant and V_a is the average atomic volume. The average wave velocity is given by v_m and is determined by the following relation:

$$v_m = \left[\frac{1}{3}\left(\frac{2}{v_t^3} + \frac{1}{v_l^3}\right)\right]^{-\frac{1}{3}} \quad (12)$$

where v_l is the longitudinal elastic wave velocity and v_t is the transverse wave velocity.

$$v_t = \left(\frac{G}{\rho}\right)^{\frac{1}{2}} \quad (13\text{-a})$$

$$v_l = \left(\frac{3B+4G}{\rho}\right)^{\frac{1}{2}} \quad (13\text{-b})$$

The elastic ductility is often accessed via Poisson's ratio (v), Pugh ratio (B/G) and Cauchy pressure ($C_{12} - C_{44}$). It is evident that the ductility is slightly enhanced with increasing Ti and V content, in terms of increase in the Poisson's ratio (v), Pugh ratio (B/G) and Cauchy pressure ($C_{12} - C_{44}$). The elastic constants, and valence electron concentration show a decreasing trend with additional amounts of Ti and V. The results indicate that the ductility of MoNbTaW alloys increases with increasing amounts of Ti and V.

4. CONCLUSIONS

This work is based on utilizing CALPHAD and first principle calculations, in conjunction with empirical rules to predict phase stability and solid-solution formation in MoNbTaW alloys woth Ti and V additions. Our calculations predict the BCC structure for $MoNbTaWV_x$(x=0-33%) and $MoNbTaWTi_x$ (x = 0−33%) to be the most stable one among the three close- packed lattices (FCC, BCC and HCP), over a wide composition range. First principles calculations based on DFT was employed to predict elastic constants of 9 different alloy compositions, to gage the effect of Ti and V on MoNbTaW based alloys. The DFT calculations utilized the supercell method for random distribution of elements in the alloy. The lattice parameters are in good agreement with available experimental data. Density of states revealed the effect of Ti and V to the electronic structure of the MoNbTaW base alloy. Although the DOS spectra for the alloys are smeared, the individual contributions of the elements to the multicomponent alloy are evidenced. The addition of Ti in increasing to the host alloy shows a shift in the peak closest to the Fermi level. Similarly, addition of V in large amounts (33 at %), shows a broadening of the peak closest to the Fermi level. The current BCC refractory alloys with Ti and V additions exhibit an increasing trend for Pugh's ratio, Poisson's ratio, and Cauchy pressure. These elastic properties all affirm that the base alloy's intrinsic ductility is improved. Since, Ti and V are less dense than Mo, Nb, Ta and W, their addition in increasing amounts will result in lighter alloys.

The raw data required to reproduce these findings are available to download from [https://data.mendeley.com/datasets/2hpznmj83h/draft?a=13fdcd5f-8f82-41ea-bc19-f836997811d7].

COMPETING INTERESTS

Authors have declared that no competing interests exist.

REFERENCES

1. Greer AL. Confusion by design. Nature; 1993.
2. Yeh JW, et al. Nanostructured high-entropy alloys with multiple principal elements: Novel alloy design concepts and outcomes. Adv. Eng. Mater; 2004.
3. Cantor B, Chang ITH, Knight P, Vincent AJB. Microstructural development in equiatomic multicomponent alloys. Mater. Sci. Eng. A; 2004.
4. Zhang Y, Zhouc YJ, Lin JP, Chen GL, Liaw PK. Solid-solution phase formation rules for multi-component alloys. Adv. Eng. Mater; 2008.
5. Takeuchi A, Amiya K, Wada T, Yubuta K, Zhang W. High-entropy alloys with a hexagonal close-packed structure designed by equi-atomic alloy strategy and binary phase diagrams. JOM; 2014.
6. Zhang Y, et al. Microstructures and properties of high-entropy alloys. Progress in Materials Science; 2014.
7. Youssef KM, Zaddach AJ, Niu C, Irving DL, Koch CC. A novel low-density, high-hardness, high-entropy alloy with close-packed single-phase nanocrystalline structures. Mater. Res. Lett; 2014.
8. Zhao K, Xia XX, Bai HY, Zhao DQ, Wang WH. Room temperature homogeneous flow in a bulk metallic glass with low glass transition temperature. Appl. Phys. Lett; 2011.
9. Gao XQ, Zhao K, Ke HB, Ding DW, Wang WH, Bai HY. High mixing entropy bulk metallic glasses. J. Non. Cryst. Solids; 2011.

10. Li HF, et al. In vitro and in vivo studies on biodegradable CaMgZnSrYb high-entropy bulk metallic glass. Acta Biomater; 2013.
11. Highmore RJ, Greer AL. Eutectics and the formation of amorphous alloys. Nature; 1989.
12. Li Y. Bulk metallic glasses: Eutectic coupled zone and amorphous formation. JOM; 2005.
13. Gludovatz B, Hohenwarter A, Catoor D, Chang EH, George EP, Ritchie RO. A fracture-resistant high-entropy alloy for cryogenic applications. Science. 2014;80.
14. Zou Y, Ma H, Spolenak R. Ultrastrong ductile and stable high-entropy alloys at small scales. Nat. Commun; 2015.
15. Zhang ZJ, et al. Nanoscale origins of the damage tolerance of the high- entropy alloy CrMnFeCoNi. Nat. Commun; 2015.
16. Liu WH et al. Ductile CoCrFeNiMox high entropy alloys strengthened by hard intermetallic phases. Acta Mater; 2016.
17. Koželj P, et al. Discovery of a superconducting high-entropy alloy. Phys. Rev. Lett; 2014.
18. Huo J, et al. The magnetocaloric effect of Gd-Tb-Dy-Al-M (M = Fe, Co and Ni) high-entropy bulk metallic glasses. /ntermetallics; 2015.
19. Huo J, et al. High-entropy bulk metallic glasses as promising magnetic refrigerants. J. Appl. Phys; 2015.
20. Chen YY, Duval T, Hung UD, Yeh JW, Shih HC. Microstructure and electrochemical properties of high entropy alloys-a comparison with type-304 stainless steel. Corros. Sci; 2005.
21. Senkov ON, Wilks GB, Miracle DB, Chuang CP, Liaw PK. Refractory high-entropy alloys. Intermetallics; 2010.
22. Senkov ON, Wilks GB, Scott JM, Miracle DB. Mechanical properties of Nb25Mo25Ta25W25 and V20Nb20Mo20Ta20W20 refractory high entropy alloys. Intermetallics; 2011.
23. Senkov ON, Scott JM, Senkova SV, Miracle DB, Woodward CF. Microstructure and room temperature properties of a high-entropy TaNbHfZrTi alloy. J. Alloys Compd; 2011.
24. Juan CC, et al. Enhanced mechanical properties of HfMoTaTiZr and HfMoNbTaTiZr refractory high-entropy alloys. Intermetallics; 2015.
25. Chen H, et al. Microstructure and mechanical properties at elevated temperatures of a new Al-containing refractory high-entropy alloy Nb-Mo-Cr-Ti-Al. J. Alloys Compd; 2016.
26. Senkov ON, Senkova SV, Woodward C, Miracle DB. Low-density, refractory multi-principal element alloys of the Cr-Nb-Ti-V-Zr system: Microstructure and phase analysis. Acta Mater; 2013.
27. Gorr B, Azim M, Christ HJ, Mueller T, Schliephake D, Heilmaier M. Phase equilibria, microstructure, and high temperature oxidation resistance of novel refractory high-entropy alloys. J. Alloys Compd; 2015.
28. Senkov ON, Semiatin SL. Microstructure and properties of a refractory high-entropy alloy after cold working. J. Alloys Compd; 2015.
29. Juan CC, et al. Solution strengthening of ductile refractory HfMoxNbTaTiZr high-entropy alloys. Mater. Lett; 2016.
30. Senkov ON, Woodward C, Miracle DB. Microstructure and Properties of Aluminum-Containing Refractory High-Entropy Alloys. JOM; 2014.
31. Senkov ON, Senkova SV, Woodward C. Effect of aluminum on the microstructure and properties of two refractory high-entropy alloys. Acta Mater; 2014.
32. Huhn WP, Widom M. Prediction of A2 to B2 phase transition in the high-entropy alloy Mo-Nb-Ta-W. JOM; 2013.
33. Yeh JW. Recent progress in high-entropy alloys. Eur. J. Control. 2006;31:633–648.
34. Wertz KN, Miller JD, Senkov ON. Toward multi-principal component alloy discovery: Assessment of CALPHAD thermodynamic databases for prediction of novel ternary alloy systems. J. Mater. Res; 2018.
35. Hohenberg P, Kohn W. Inhomogeneous electron gas. Phys. Rev; 1964.
36. Kresse G. Ab initio molecular dynamics for liquid metals. J. Non. Cryst. Solids; 1995.
37. Ganesh P, Widom M. Ab initio simulations of geometrical frustration in supercooled liquid Fe and Fe-based metallic glass. Phys. Rev. B - Condens. Matter Mater. Phys; 2008.
38. Chizmeshya AVG, Bauer MR, Kouvetakis J. Experimental and theoretical study of deviations from Vegard's law in the SnxGe1-x system. Chem. Mater; 2003.
39. Soven P. Coherent-potential model of substitutional disordered alloys. Phys. Rev; 1967.
40. Zaddach AJ, Niu C, Koch CC, Irving DL. Mechanical properties and stacking fault

energies of NiFeCrCoMn high-entropy alloy. JOM; 2013.
41. Bellaiche L, Vanderbilt D. Virtual crystal approximation revisited: Application to dielectric and piezoelectric properties of perovskites. Phys. Rev. B-Condens. Matter Mater. Phys; 2000.
42. Guo S, Ng C, Lu J, Liu CT. Phase equilibria, microstructure, and high temperature oxidation resistance of novel refractory high-entropy alloys. J. Alloys Compd. in Journal of Applied Physics. 2011;624(2015):270e278.
43. Troparevsky MC, Morris JR, Kent PRC, Lupini AR, Stocks GM. Criteria for predicting the formation of single-phase high-entropy alloys. Phys. Rev. X; 2015.
44. Zhang F, Zhang C, Chen SL, Zhu J, Cao WS, Kattner UR. An understanding of high entropy alloys from phase diagram calculations. Calphad Comput. Coupling Phase Diagrams Thermochem; 2014.
45. Senkov ON, Miller JD, Miracle DB, Woodward C. Accelerated exploration of multi-principal element alloys with solid solution phases. Nat. Commun; 2015.
46. Senkov ON, Miller JD, Miracle DB, Woodward C. Accelerated exploration of multi-principal element alloys for structural applications. Calphad Comput. Coupling Phase Diagrams Thermochem; 2015.
47. Gorsse S, Senkov ON. About the reliability of CALPHAD predictions in multi component systems. Entropy; 2018.
48. Yao HW, Qiao JW, Hawk JA, Zhou HF, Chen MW, Gao MC. Mechanical properties of refractory high-entropy alloys: Experiments and modeling. J. Alloys Compd; 2017.
49. Han ZD, et al. Effect of Ti additions on mechanical properties of NbMoTaW and VNbMoTaW refractory high entropy alloys. Intermetallics; 2017.
50. Sundman B, Jansson B, Andersson JO. The Thermo-Calc databank system Le système de banque de données Thermo-Calc. Calphad; 1985.
51. King DJM, Middleburgh SC, McGregor AG, Cortie MB. Predicting the formation and stability of single phase high-entropy alloys. Acta Mater; 2016.
52. Middleburgh SC, King DM, Lumpkin GR, Cortie M, Edwards L. Segregation and migration of species in the CrCoFeNi high entropy alloy. Journal of Alloys and Compounds; 2014.
53. Blaha JLP, Schwarz K, Madsen GKH, Kvasnicka D. An augmented plane wave+local orbitals program for calculating crystal properties. Techn. Univ. Wien, Austria; 2001.
54. Hill R. The elastic behaviour of a crystalline aggregate. Proc. Phys. Soc. Sect. A; 1952.
55. Voigt W. Lehrbuch der Kristallphysik; 2013.
56. Reuss A. Berechnung der Fließgrenze von Mischkristallen auf Grund der Plastizitätsbedingung für Einkristalle. ZAMM - J. Appl. Math. Mech. / Zeitschrift für Angew. Math. und Mech; 1929.
57. Pugh SF. XCII. Relations between the elastic moduli and the plastic properties of polycrystalline pure metals. London, Edinburgh, Dublin Philos. Mag. J. Sci; 1954.
58. Pettifor DG. Theoretical predictions of structure and related properties of intermetallics. Mater. Sci. Technol; 2014.

Peer-review history:
The peer review history for this paper can be accessed here:
http://www.sdiarticle4.com/review-history/52208